Stochastic Response Analysis and Reliability-Based Design Optimization of Nonlinear Electromechanical Energy Harvesters With Fractional Derivative Elements

Ioannis Petromichelakis
Department of Civil Engineering and Engineering Mechanics,
Columbia University,
500 W. 120th Street,
New York, NY 10027
e-mail: ip2315@columbia.edu

Apostolos F. Psaros
Department of Civil Engineering and Engineering Mechanics,
Columbia University,
500 W. 120th Street,
New York, NY 10027

Ioannis A. Kougioumtzoglou
Department of Civil Engineering and Engineering Mechanics,
Columbia University,
500 W. 120th Street,
New York, NY 10027

A methodology based on the Wiener path integral (WPI) technique is developed for stochastic response determination and reliability-based design optimization of a class of nonlinear electromechanical energy harvesters endowed with fractional derivative elements. In this regard, first, the WPI technique is appropriately adapted and enhanced to account both for the singular diffusion matrix and for the fractional derivative modeling of the capacitance in the coupled electromechanical governing equations. Next, a reliability-based design optimization problem is formulated and solved, in conjunction with the WPI technique, for determining the optimal parameters of the harvester. It is noted that the herein proposed definition of the failure probability constraint is particularly suitable for harvester configurations subject to space limitations. Several numerical examples are included, while comparisons with pertinent Monte Carlo simulation (MCS) data demonstrate the satisfactory performance of the methodology.
[DOI: 10.1115/1.4049232]

1 Introduction

A large class of energy harvesters exploit the ability of active materials (e.g., piezoelectric) and electromechanical coupling mechanisms to generate an electric potential in response to external excitations. Utilizing an appropriate circuit, the electric potential is converted into current, and thus, mechanical energy is transformed into electrical. Following early efforts referring to linear system modeling (e.g., Refs. [1–3]), researchers intentionally considered nonlinear designs (e.g., via appropriate placement of magnets) for increasing the coupling range between the excitation and the system, and therefore, for enhancing the efficiency and energy output of the harvester (e.g., Refs. [4] and [5]).

Further, many energy harvesters operate in tandem with structures and civil infrastructure systems, which are subjected to environmental excitations that have random and even time-varying characteristics. Thus, researchers have recently realized the need for modeling the excitations as stochastic processes [6–10]. Moreover, it has been shown that experimentally collected impedance data related to various energy storage systems can be best represented by fractional derivative modeling (e.g., Refs. [11] and [12]). In this regard, there have been efforts to propose enhanced versions of the energy harvester coupled electromechanical equations by incorporating fractional derivative elements (e.g., Refs. [13] and [14]).

Regarding design and optimization of energy harvesters for maximizing energy output, this has been done primarily by considering deterministic harmonic excitations (e.g., Ref. [15]), whereas the few papers referring to stochastic excitations employ almost exclusively the maximization of mean harvested power as the optimization criterion [16–18]. However, as also highlighted in Refs. [19] and [20], it is clear that consideration of additional restrictions and constraints related to low probability events is necessary for avoiding, for instance, equipment failures. Such constraints may relate to the probability that the voltage and/or the displacement stay within prescribed limits, while their inclusion in the energy harvester optimization problem can lead, potentially, to a more robust and efficient design than what is currently the norm; see also Ref. [20] for a more detailed discussion. Thus, advanced stochastic dynamics techniques are required, capable of determining the joint response probability density function (PDF) to be used in the constrained optimization problem of such energy harvesting systems. Obviously, utilization of approximate techniques, such as the widely employed standard statistical linearization [18,21,22], which yield only first- and second-order response statistics (i.e., mean and standard deviation) is inadequate for optimization subject to low probability constraints.

In this paper, a methodology based on the Wiener path integral (WPI) technique (e.g., Refs. [23–27]) is developed for stochastic response analysis and optimization of a class of energy harvesters exhibiting asymmetric nonlinearities and endowed with fractional derivative elements. Specifically, the WPI technique is appropriately adapted herein to be used in conjunction with a constrained optimization algorithm for determining efficiently the optimal parameters of the energy harvester. The paper can be construed as an extension of the work in Ref. [20] to account for fractional derivative terms in the governing equations. Further, in comparison to Ref. [20], the overall complexity of the constrained optimization problem is increased not only because of the more sophisticated modeling based on fractional derivatives but also due to considering an augmented higher dimensional vector of optimization variables. Moreover, regarding the reliability-based probabilistic constraint, which is considered in the optimization problem, a rather pragmatic definition is proposed herein for cases referring to space limitations. Several numerical examples are included, while comparisons with pertinent Monte Carlo simulation (MCS) data demonstrate the reliability and robustness of the methodology.

Manuscript received December 16, 2019; final manuscript received December 1, 2020; published online January 21, 2021. Assoc. Editor: Agathoklis Giaralis.

2 Nonlinear Electromechanical Energy Harvester With Fractional Derivative Elements

2.1 Modeling aspects. One of the most widely studied electromechanical energy harvesters consists of a cantilever beam with piezoelectric patches attached near its clamped ends as shown in Fig. 1(*a*). The vibrating beam induces strain to the piezoelectric patches, and thus, electrical voltage is generated and energy is harvested with the aid of an electrical circuit connected to the patches. It has been shown experimentally [8,28,29] that intentional incorporation of system nonlinearities, typically realized by appropriate installation of magnets as shown in Fig. 1(*a*), can potentially increase the harvested energy. This has been also verified numerically in several studies [5,30,31] in conjunction with a Duffing model to describe the mechanical nonlinearities. As discussed in detail in Ref. [5], the dynamics of such a system (see Fig. 1(*a*)) can be approximated by the following general mathematical model of coupled electromechanical equations, expressed in a nondimensional form as

$$\ddot{x} + 2\zeta\dot{x} + \frac{dU(x)}{dx} + \kappa^2 y = w(t) \tag{1a}$$

$$\dot{y} + \alpha y - \dot{x} = 0 \tag{1b}$$

where x denotes the response displacement and y represents the induced voltage in capacitative harvesters or the induced current in inductive ones. Further, ζ is the damping, κ is the coupling coefficient, α (referred to as the electrical constant in the following) is defined as the ratio between the mechanical and electrical time constants of the harvester (see Ref. [21]), and $U(x)$ denotes the potential function. Its derivative $dU(x)/dx$ represents the restoring force, which is nonlinear in general; see Ref. [5] for more details. Also, $w(t)$ represents the external excitation, which is modeled as a Gaussian white noise stochastic process with a constant power spectrum value S_0. Details regarding the nondimensionalization of the governing equations can be found in Refs. [21] and [32].

In modeling the restoring force $dU(x)/dx$, a wide range of nonlinear behaviors can be captured by the third-order polynomial

$$\frac{dU(x)}{dx} = x + \lambda x^2 + \delta x^3 \tag{2}$$

where λ and δ control the intensity of the quadratic and cubic nonlinear terms, respectively, while the coefficient corresponding to the linear stiffness term equals 1 as a result of the nondimensionalization [21]. Further, considering the behavior of the potential function $U(x)$ for $\delta \geq 0$ (see Fig. 1(*b*)), Eq. (2) leads to a bistable asymmetric potential for $\lambda > 2\sqrt{\delta}$ (dashed-dotted line), to a monostable asymmetric potential for $0 < \lambda \leq 2\sqrt{\delta}$ (dashed line), and to a monostable symmetric potential for $\lambda = 0$ (dotted line).

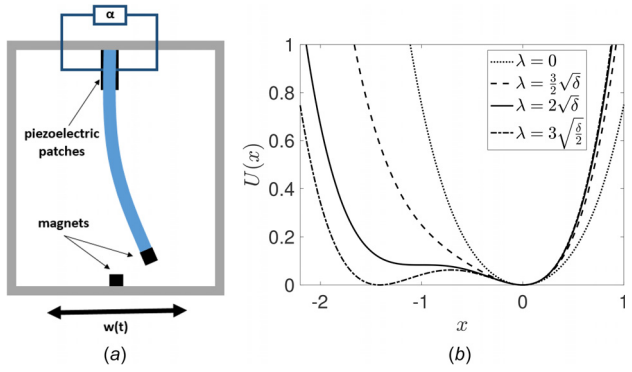

Fig. 1 (*a*) Schematic representation of the electromechanical energy harvesting device. (*b*) Various shapes of the potential function for $\delta = 1$.

As shown in Ref. [21], for $\lambda = 0$ and Gaussian white noise excitation, the maximum mean harvested power is achieved for $\delta = 0$, or in other words, the linear system is optimal; see also Refs. [31] and [33–35] for a relevant discussion on the optimality of linear systems under certain conditions. Furthermore, it was shown in Refs. [22] and [32] that utilizing nonlinear oscillators with symmetric bistable potentials, i.e., $\lambda = 0$ and a restoring force of the form $dU(x)/dx = -x + \delta x^3$, can be beneficial for maximizing the mean harvested power. In this regard, a question is posed naturally regarding the performance, in terms of harvesting efficiency, of potential functions with asymmetries, i.e., $\lambda \neq 0$. This was addressed in Refs. [21] and [36] where the response statistics of monostable harvesters in the regime $0 \leq \lambda \leq 2\sqrt{\delta}$ were determined via statistical linearization. It was shown that the maximum mean harvested power is achieved for some $\delta > 0$ and for the bistability limit $\lambda = 2\sqrt{\delta}$ (solid line in Fig. 1(*b*)).

Further, it can be argued that models of electric circuits involving fractional derivative terms are, in general, in better agreement with experimental data than their traditionally used integer order counterparts. In fact, it has been shown that experimentally collected impedance data from a variety of energy storage systems (e.g., supercapacitors) can be best represented by fractional order models (e.g., Refs. [11] and [12]).

Although there have been few recent research efforts to provide an enhanced version of Eq. (1) by incorporating fractional derivative terms in the electrical Eq. (1*a*) (e.g., Refs. [13] and [14]), these have been either limited to considering cases of deterministic excitation only, or restricted to system response analysis without proposing any efficient optimization framework. In this paper, a class of nonlinear electromechanical energy harvesters with fractional order derivatives in the electrical equation and parameter $\lambda \leq 2\sqrt{\delta}$, with $\delta \geq 0$ (i.e., monostable asymmetric system) is considered. These systems are characterized by a single equilibrium position at $(x, y) = (0, 0)$. Following Ref. [14] for the fractional derivative modeling of the capacitance, the coupled electromechanical system of equations takes the general form

$$\ddot{x} + 2\zeta\dot{x} + x + \lambda x^2 + \delta x^3 + \kappa^2 y = w(t) \tag{3a}$$

$$D^r y + \alpha y - \dot{x} = 0 \tag{3b}$$

where D^r is the rth order fractional derivative operator, defined as

$$D^r[f(t)] = \frac{d^r f}{dt^r} = \frac{1}{\Gamma(1-r)} \int_{t_i}^{t} \frac{\dot{f}(\tau)}{(t-\tau)^r} \mathrm{d}\tau \tag{4}$$

Equation (4) represents a Caputo fractional derivative of order $0 < r < 1$ (see also Ref. [37] for alternative fractional derivative definitions). Note that in the limit $r \to 1$, Eq. (3*b*) degenerates to Eq. (1*b*). Next, to provide some insight regarding the dynamics of the system of Eq. (3), Eq. (3*a*) can be construed as the governing stochastic differential equation (SDE) constrained by the fractional differential equation of Eq. (3*b*). The system response vector process $\boldsymbol{q} = [x, \dot{x}, y]^T$ starts from initial conditions, exhibits a transient phase, and eventually reaches stationarity where the maximum response variance is observed. In this regard, the mean harvested power P_h is proportional to the stationary variance of the zero-mean electrical quantity y, and is given by (e.g., Ref. [5])

$$P_h = \alpha \mathbb{E}\{y^2\} \tag{5}$$

where $\mathbb{E}\{.\}$ represents the expectation operator. It is noted that in comparison with Ref. [20], not only the complexity of the governing equations (Eq. (1)) is increased by considering fractional derivative terms, but also the range of harvester design configurations to be studied herein is extended by allowing $\lambda \leq 2\sqrt{\delta}$ (unlike $\lambda = 2\sqrt{\delta}$ used in Ref. [20]).

2.2 Optimization Aspects. From an optimal design perspective, the objective is typically expressed in the literature as

maximizing the mean stationary harvested power P_h for a given excitation intensity S_0. This can be formulated as an optimization problem in the set of parameters $\{\zeta, \delta, \lambda, \kappa, \alpha\} \subseteq \mathbb{R}_+^5$, where $\mathbb{R}_+$ denotes the set of positive real numbers. Nevertheless, the complexity of the problem can be decreased by examining the impact of parameter κ on the system dynamics. Specifically, considering Eqs. (1) and (5), it is seen that a larger coupling coefficient κ yields a larger variance of the electrical quantity y in a monotonic manner. As a result, κ should take the largest value possible, and thus, can be excluded from the optimization problem. The rest of the parameters affect the output harvested power in a more complex manner (see also Ref. [20] for a relevant discussion). Therefore, they need to be included in the optimization. In this regard, for the parameter vector $\boldsymbol{z} = [\alpha, \delta, \zeta, \lambda]$ and for κ and S_0 fixed, the harvester design problem can be formulated as an optimization problem of the form

$$\arg\max_{z \in Z} P_h(\boldsymbol{z}) \tag{6}$$

where $Z \subset \mathbb{R}_+^4$ is an effective domain of parameter values.

Nevertheless, additional design criteria need to be considered in practice, which translate into constraints to be enforced. Such constraints can take the general form $P_f(\boldsymbol{z}) < \epsilon$, where the probability of failure P_f refers typically to an "extreme event" characterized by a low probability of occurrence. Indicatively, excessively high voltage levels, or extreme displacement values, may compromise the proper function of the electronic circuits, or may cause mechanical failure to the oscillator, respectively. In such cases, P_f can be defined as the probability that either $|x|$ or $|y|$ exceed some prescribed limit, i.e., $P_f = P(|x| > x_{\text{limit}} \text{ or } |y| > y_{\text{limit}})$. Taking such an additional design criterion into account, Eq. (6) is reformulated as a reliability-based optimization problem in the form

$$\arg\max_{z \in Z} P_h(\boldsymbol{z}) \quad \text{s.t.} \quad P_f(\boldsymbol{z}) \leq \epsilon \tag{7}$$

Note, however, that if failure is defined as $|x| > x_{\text{limit}}$, the imposed limits on the displacement x are symmetric with respect to the equilibrium position $x = 0$. Although this may be a reasonable constraint definition for cases referring, for instance, to mechanical failures due to excessive levels of displacement, it is problematic when addressing the challenge of limited available space for the harvester. Specifically, it can be readily seen that since the herein considered harvesting system is asymmetric, employing such a failure definition does not exploit fully the available space; thus, leading potentially to an unnecessarily conservative design. In this regard, a more pragmatic approach regarding the failure criterion for such cases is proposed in the following. This relates to considering a box of specific width L_b, and to defining the probability of failure as the smallest probability of exceeding either end of the box for all possible locations of the harvester within the box. This is represented graphically and explained in Fig. 2(*a*), which depicts the stationary marginal PDF of the response displacement x of a typical asymmetric harvester, positioned at two different locations within a box of width L_b. The thin solid curve denotes the PDF of the harvester with equilibrium position at $x = 0$, leading to a probability of failure $P_{f,1}$ (shaded region under thin solid curve). This configuration can be found by utilizing a constraint on the probability of failure of the form $P_f = P(|x| > x_{\text{limit}}) < \epsilon$ with $x_{\text{limit}} = (L_b/2)$. Further, the thick solid curve in Fig. 2(*a*), represents the PDF of the same harvester, shifted by δx to the right to yield an overall lower probability of failure $P_{f,2} < P_{f,1}$ (shaded region under thick solid curve). Thus, from a practical perspective, the optimal design of an asymmetric harvester subject to limited available space should, ideally, specify the location of the device (or more specifically, the location of its equilibrium position) within the box so that the probability of failure is minimized (see Fig. 2(*b*)). This is typically achieved when P_f is "shared" by both tails in an optimal manner. In other words, the harvester should be placed within the box in a manner that exploits fully the available space for a given box width L_b.

In this regard, the location of a harvester's equilibrium position within the box, i.e., the shift parameter δx, needs to be considered as an additional unknown variable to be determined. Thus, the design optimization problem in Eq. (7) is adapted by considering the augmented variable vector $\bar{\boldsymbol{z}} = [\boldsymbol{z}, \delta x] = [\alpha, \delta, \zeta, \lambda, \delta x]$ and by defining the probability of failure P_f as

$$P_f(\bar{\boldsymbol{z}}) = 1 - S_z(\delta x) \tag{8}$$

where

$$S_z(u) = \int_{-\infty}^{\infty} \text{rect}\left(\frac{v}{L_b}\right) p_{z,s}(v+u)\mathrm{d}v \tag{9}$$

represents the survival probability and rect(.) is a rectangular pulse function defined as

$$\text{rect}(x) = \begin{cases} 0, & \text{if } |x| > \dfrac{1}{2} \\ \dfrac{1}{2}, & \text{if } |x| = \dfrac{1}{2} \\ 1, & \text{if } |x| < \dfrac{1}{2} \end{cases} \tag{10}$$

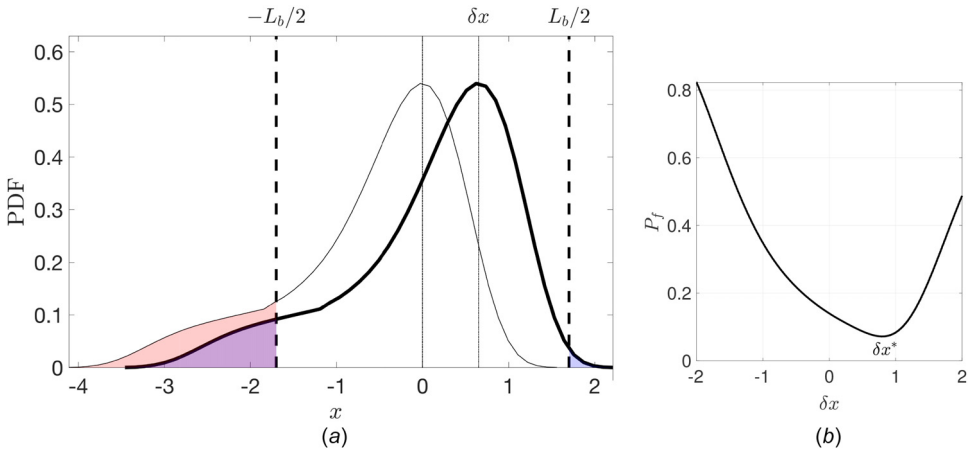

Fig. 2 Impact of the harvester location δx within a box of width L_b on the probability of failure P_f. (*a*) Stationary marginal PDFs of the response displacement x. *Thin solid curve*: $\delta x = 0$ yielding $P_{f,1}$. *Thick solid curve*: $\delta x > 0$ yielding $P_{f,2} < P_{f,1}$. (*b*) Relationship between δx and P_f, depicting a well-defined optimal position.

Also, Fig. 2(*b*) shows a typical behavior of Eq. (8) with respect to δx.

However, a closer examination of the objective function in Eq. (7), reveals that this depends only on $\boldsymbol{z}$, i.e., the variables α, δ, ζ, and λ, whereas δx is involved only in the constraint. Moreover, for a given set of values $\boldsymbol{z}$, the optimal location δx^*, i.e., the one corresponding to minimal probability of failure, can be determined simply as

$$\delta x^* = \arg \max_u S_z(u) \tag{11}$$

From a numerical optimization perspective, this enables the evaluation of the vector $\boldsymbol{z}$ at each iteration step independently of δx, followed by the estimation of the optimal δx^* by solving the rather trivial (one-dimensional) problem of Eq. (11). In other words, the optimization problem considers effectively only the four variables of vector $\boldsymbol{z}$ to be optimized simultaneously at each iteration, whereas the optimal location δx^* is provided essentially as a by-product. Thus, the complexity of the optimization problem relates, essentially, to a four-dimensional problem involving $\boldsymbol{z}$, such as in Eq. (7) (as opposed to an augmented five-dimensional problem involving $\bar{\boldsymbol{z}}$), whereas considering (11), Eq. (8) is written as

$$P_f(\boldsymbol{z}) = 1 - \max_{\boldsymbol{u}} S_z(\boldsymbol{u}) \tag{12}$$

Further, a penalty approach is utilized herein for solving the constrained problem of Eq. (7). This yields an unconstrained problem with the modified objective function $P_{h,\epsilon}(\boldsymbol{z}) = \mathbb{1}_\epsilon(\boldsymbol{z})P_h(\boldsymbol{z})$, where 1_ϵ is an indicator function defined as

$$\mathbb{1}_\epsilon(\boldsymbol{z}) = \begin{cases} 0, & P_f(\boldsymbol{z}) \geq \epsilon \\ 1, & \text{otherwise} \end{cases} \tag{13}$$

Considering that information regarding the gradient of the objective function $P_h(\boldsymbol{z})$ related to Eq. (7) is not available in general, the extended gradient-free generalized pattern search (GPS) optimization algorithm is utilized next, which requires no assumptions about the differentiability and continuity of the objective function [38–40].

Obviously, knowledge of the harvester complete response PDF is required to be used in the optimization procedure, and not only of the response mean and variance that are typically determined in the literature. To this aim, the WPI stochastic response determination technique is adapted and applied herein in conjunction with the constrained optimization problem of Eq. (7). In comparison with Ref. [20], a more pragmatic version of the reliability-based constraints referring to space limitations is considered in Eq. (12), while the overall complexity of the optimization problem is increased. This is not only because of a more sophisticated modeling of Eqs. (1) based on fractional derivatives, but also due to considering a higher dimensional vector $\boldsymbol{z}$; that is, five optimization variables (i.e., $[\alpha, \zeta, \lambda, \delta]$ and δx) are considered herein in contrast to the two variables in Ref. [20]. Hereinafter, the explicit dependence of a stationary marginal response PDF on $\boldsymbol{z}$ is suppressed for simplicity and $p_{z,s}(.)$ is denoted as $p_s(.)$.

3 Wiener Path Integral Solution Technique Overview

The WPI technique has been recently pioneered and developed in the field of engineering dynamics for determining the stochastic response of diverse dynamic systems, including multidegree-of-freedom structures exhibiting various nonlinear behaviors, even endowed with fractional derivative terms and subject to non-Gaussian and nonwhite excitations [23–27,41,42]. A significant advantage of the technique relates to the fact that it exhibits both relatively high accuracy and reasonable computational cost in determining the joint response transition PDF, especially when coupled with sparse representations and compressive sampling concepts and tools [25,41,43]. In passing, it is noted that the WPI technique, which is based on a variational formulation, should not be confused with alternative numerical path integration schemes (see, e.g., Refs. [44] and [45]). Concisely, the latter constitute discrete versions of the Chapman–Kolmogorov equation, which utilize an appropriately chosen short-time transition PDF for advancing in time the system joint response PDF. Although these schemes exhibit excellent accuracy in determining even the tails of the response PDF, they become eventually computationally prohibitive with increasing dimensionality.

For completeness, the salient aspects of the technique are delineated in the present section by considering the general class of n-dimensional randomly excited systems whose dynamics is described by

$$\boldsymbol{D}[\boldsymbol{q}(t)] = \boldsymbol{w}(t) \tag{14}$$

In Eq. (14), $\boldsymbol{D}[.]$ denotes a nonlinear, in general, differential operator with second being the highest order derivative involved according to the standard modeling of structural/mechanical systems. Further, $\boldsymbol{q}$ is the system response, and $\boldsymbol{w}$ is a white noise stochastic excitation vector process with $E[\boldsymbol{w}(t_1)\boldsymbol{w}(t_2)] = \boldsymbol{B}\delta(t_2 - t_1)$; $\delta(.)$ denotes the Dirac delta function and $\boldsymbol{B}$ is a deterministic coefficient matrix given by

$$\boldsymbol{B} = \begin{bmatrix} 2\pi S_0 & \dots & 0 \\ \vdots & \ddots & \vdots \\ 0 & \dots & 2\pi S_0 \end{bmatrix} \tag{15}$$

Next, relying on the mathematical framework of path integrals [46], the response transition PDF $p(\boldsymbol{q}_f, \dot{\boldsymbol{q}}_f, t_f | \boldsymbol{q}_i, \dot{\boldsymbol{q}}_i, t_i)$ can be written as [24]

$$p(\boldsymbol{q}_f, \dot{\boldsymbol{q}}_f, t_f | \boldsymbol{q}_i, \dot{\boldsymbol{q}}_i, t_i) = \int_{\mathcal{C}\{\boldsymbol{q}_i, \dot{\boldsymbol{q}}_i, t_i; \boldsymbol{q}_f, \dot{\boldsymbol{q}}_f, t_f\}} \exp\left(- \int_{t_i}^{t_f} \mathcal{L}(\boldsymbol{q}, \dot{\boldsymbol{q}}, \ddot{\boldsymbol{q}}) \mathrm{d}t \right) [\mathrm{d}\boldsymbol{q}(t)] \tag{16}$$

with $\{\boldsymbol{q}_i, \dot{\boldsymbol{q}}_i, t_i\}$ denoting the initial state and $\{\boldsymbol{q}_f, \dot{\boldsymbol{q}}_f, t_f\}$ the final state, and $\boldsymbol{q}_i = \boldsymbol{q}(t_i)$, $\boldsymbol{q}_f = \boldsymbol{q}(t_f)$, $\dot{\boldsymbol{q}}_i = \dot{\boldsymbol{q}}(t_i)$, and $\dot{\boldsymbol{q}}_f = \dot{\boldsymbol{q}}(t_f)$. Equation (16) represents a functional integral over the space of all possible paths $\mathcal{C}\{\boldsymbol{q}_i, \dot{\boldsymbol{q}}_i, t_i; \boldsymbol{q}_f, \dot{\boldsymbol{q}}_f, t_f\}$, with $[\mathrm{d}\boldsymbol{q}(t)]$ being a functional measure [46] and $\mathcal{L}(\boldsymbol{q}, \dot{\boldsymbol{q}}, \ddot{\boldsymbol{q}})$ denoting the Lagrangian functional expressed as [24]

$$\mathcal{L}(\boldsymbol{q}, \dot{\boldsymbol{q}}, \ddot{\boldsymbol{q}}) = \frac{1}{2} \boldsymbol{D}[\boldsymbol{q}]^T \boldsymbol{B}^{-1} \boldsymbol{D}[\boldsymbol{q}] \tag{17}$$

In general, analytical evaluation of the functional integral of Eq. (16) is not possible. To address this challenge, one of the most typically used approximate techniques relates to considering only the largest contribution to the functional integral. This comes from the trajectory $\boldsymbol{q}_c(t)$ for which the integral in the exponential of Eq. (16) (also known as stochastic action) becomes as small as possible (e.g., Ref. [46]). In this regard, the determination of the n-dimensional most probable path $\boldsymbol{q}_c(t)$ is formulated as a variational problem (functional minimization) of the form

$$\text{minimize } \mathcal{J}(\boldsymbol{q}) = \int_{t_i}^{t_f} \mathcal{L}(\boldsymbol{q}, \dot{\boldsymbol{q}}, \ddot{\boldsymbol{q}}) \mathrm{d}t \tag{18}$$

Subject to the set of boundary conditions

$$\begin{aligned} q_j(t_i) &= q_{j,i} \quad \dot{q}_j(t_i) = \dot{q}_{j,i} \\ q_j(t_f) &= q_{j,f} \quad \dot{q}_j(t_f) = \dot{q}_{j,f} \qquad j = 1, \dots, n \end{aligned} \tag{19}$$

Following determination of $\boldsymbol{q}_c(t)$, a specific point of the system response transition PDF is evaluated as [24]

$$p(\boldsymbol{q}_f, \dot{\boldsymbol{q}}_f, t_f | \boldsymbol{q}_i, \dot{\boldsymbol{q}}_i, t_i) \approx C \exp\left(- \int_{t_i}^{t_f} L(\boldsymbol{q}_c, \dot{\boldsymbol{q}}_c, \ddot{\boldsymbol{q}}_c) \mathrm{d}t \right) \tag{20}$$

In Eq. (20), the normalization constant C is computed by utilizing the condition

$$\int_{-\infty}^{\infty} \dots \int_{-\infty}^{\infty} p(\boldsymbol{q}_f, \dot{\boldsymbol{q}}_f, t_f | \boldsymbol{q}_i, \dot{\boldsymbol{q}}_i, t_i) \mathrm{d}x_{1f} \mathrm{d}\dot{x}_{1f} \dots \mathrm{d}x_{mf} \mathrm{d}\dot{x}_{mf} = 1 \tag{21}$$

4 Adaptation of the Wiener Path Integral Technique to Address the Nonlinear Electromechanical Harvester With Fractional Derivative Terms

4.1 Theoretical Aspects. Considering Eq. (3), it can be readily seen that a straightforward application of Eq. (17) would lead to a singular matrix $\boldsymbol{B}$. Thus, a modification is required to the WPI technique presented in Sec. 3 to account for the special form of Eq. (3). In the ensuing analysis, Eq. (3*a*) is construed as an underdetermined SDE with two unknown functions ($x(t)$ and $y(t)$), excited by the Gaussian white noise process $w(t)$. Setting $\boldsymbol{q} = [x, y]^T$, the corresponding Lagrangian is expressed as

$$\begin{aligned} \mathcal{L}(\boldsymbol{q}, \dot{\boldsymbol{q}}, \ddot{\boldsymbol{q}}) &= \mathcal{L}(x, y, \dot{x}, \ddot{x}) \\ &= \frac{1}{4\pi S_0} \left[\ddot{x} + 2\zeta \dot{x} + x + \lambda x^2 + \delta x^3 + \kappa^2 y \right]^2 \end{aligned} \tag{22}$$

Next, to account also for the impact of Eq. (1*b*) on the harvester dynamics, Eq. (1*b*) is treated as a dynamic constraint in the form

$$\phi(y, D^r y, \dot{x}) = D^r y + \alpha y - \dot{x} = 0 \tag{23}$$

Equation (22) in conjunction with Eq. (23) lead to a fractional constrained variational problem of the form

$$\begin{aligned} &\text{minimize } \mathcal{J}(x,y,\dot{x},\ddot{x}) = \int_{t_i}^{t_f} \mathcal{L}(x,y,\dot{x},\ddot{x}) \mathrm{d}t \\ &\text{subject to } \phi(y, D^r y, \dot{x}) = 0 \end{aligned} \tag{24}$$

with the boundary conditions

$$\begin{aligned} &x(t_i) = x_i, \quad \dot{x}(t_i) = \dot{x}_i, \quad y(t_i) = y_i \\ &x(t_f) = x_f, \quad \dot{x}(t_f) = \dot{x}_f, \quad y(t_f) = y_f \end{aligned} \tag{25}$$

In the Sec. 4.2, the numerical solution of Eqs. (24) and (25) is determined by formulating and employing a constrained optimization numerical scheme (e.g., Ref. [47]).

4.2 Numerical Aspects. In this section, a Rayleigh–Ritz direct minimization approach is proposed for solving the constrained variational problem of Eqs. (24) and (25), and for determining the most probable path $\boldsymbol{q}_c(t) = [x_c(t), y_c(t)]^T$.

In this regard, the standard Rayleigh–Ritz approach relies on an expansion for $\boldsymbol{q}(t)$ in the form $\boldsymbol{q}(t) \approx \hat{\boldsymbol{q}}(t) = \boldsymbol{\psi}(t) + \boldsymbol{C}\boldsymbol{h}(t)$, where $\boldsymbol{h}(t) = [h_0(t), \dots, h_{L-1}(t)]^T$ is a basis of polynomial functions vanishing at the boundaries, $\boldsymbol{\psi}(t) = [\psi_1(t), \dots, \psi_n(t)]^T$ is a vector of n polynomials satisfying the boundary conditions and $\boldsymbol{C} \in \mathbb{R}^{n \times L}$ is the expansion coefficient matrix. Obviously, since this expansion satisfies the boundary conditions by construction, the functional minimization problem of Eqs. (18) and (19) can be directly reformulated as an unconstrained optimization problem over the space of the coefficients $\boldsymbol{C}$. Note, however, that in the herein developed formulation, in addition to the boundary conditions of Eq. (25), the dynamic constraint of Eq. (23) needs to be accounted for as well. Thus, a standard implementation of the Rayleigh–Ritz approach would lead, unavoidably, to an overall constrained optimization problem (e.g., Ref. [20]). In this regard, an alternative formulation of the optimization problem is proposed next, which accounts for the boundary conditions and the dynamic constraint in a more direct and straightforward manner. Specifically, a standard polynomial expansion for $\boldsymbol{q}(t) = [x(t), y(t)]^T$ is adopted, which takes the form

$$\begin{bmatrix} \bar{x}(t) \\ \bar{y}(t) \end{bmatrix} = \boldsymbol{C}\boldsymbol{g}(t) = [\, \boldsymbol{c}_x \quad \boldsymbol{c}_y \,]^T \boldsymbol{g}(t) \tag{26}$$

where $\boldsymbol{g}(t) = [g_0(t), \dots, g_{L-1}(t)]^T$ is a basis of polynomial functions that are orthogonal in the interval $[t_i, t_f]$. In the ensuing analysis, the shifted Legendre polynomials given by the recursive formula

$$g_{p+1}(t) = \frac{2p+1}{p+1} \left(\frac{2t - t_i - t_f}{t_f - t_i} \right) g_p(t) - \frac{p}{p+1} g_{p-1}(t), \quad p = 1, 2, \dots \tag{27}$$

are employed, with $g_0(t) = 1$; and $g_1(t) = (2t - t_i - t_f)/(t_f - t_i)$. Next, the first and second derivatives of $x(t)$ are expressed as $\dot{\bar{x}} = \boldsymbol{c}_x \dot{\boldsymbol{g}}$ and $\ddot{\bar{x}} = \boldsymbol{c}_x \ddot{\boldsymbol{g}}$, respectively, and thus, the functional $\mathcal{J}(x, y, \dot{x}, \ddot{x})$ in Eq. (24) is approximated by the function

$$J(\boldsymbol{c}) = \mathcal{J}(\bar{x}, \bar{y}, \dot{\bar{x}}, \ddot{\bar{x}}) \tag{28}$$

where $\boldsymbol{c} = [\, \boldsymbol{c}_x^T \quad \boldsymbol{c}_y^T \,]^T \in \mathbb{R}^{2L}$ is the vectorized form of $\boldsymbol{C} \in \mathbb{R}^{2 \times L}$. Moreover, the fractional order derivative of $y(t)$ is expressed as

$$D^r \bar{y} = \boldsymbol{c}_y D^r \boldsymbol{g} \tag{29}$$

where $D^r \boldsymbol{g} = \{D^r[g_0(t)], \dots, D^r[g_{L-1}(t)]\}^T$ is the vector of fractional derivatives of the L polynomial basis functions.

Clearly, compared to the classical Rayleigh–Ritz method, $[\bar{x}(t), \bar{y}(t)]^T$ in the expansion of Eq. (26) does not necessarily satisfy the boundary conditions of Eq. (25). To address this point, the initial and final boundary conditions of Eq. (25) are imposed explicitly as linear constraints of the form

$$\begin{aligned} \boldsymbol{A}_i \boldsymbol{c} &= \boldsymbol{b}_i \\ \boldsymbol{A}_f \boldsymbol{c} &= \boldsymbol{b}_f \end{aligned} \tag{30}$$

where the matrices $\boldsymbol{A}_i, \boldsymbol{A}_f \in \mathbb{R}^{3 \times 2L}$ are given by

$$\boldsymbol{A}_i = \begin{bmatrix} \boldsymbol{g}(t_i)^T & \boldsymbol{0} \\ \boldsymbol{0} & \boldsymbol{g}(t_i)^T \\ \dot{\boldsymbol{g}}(t_i)^T & \boldsymbol{0} \end{bmatrix} \quad \text{and} \quad \boldsymbol{A}_f = \begin{bmatrix} \boldsymbol{g}(t_f)^T & \boldsymbol{0} \\ \boldsymbol{0} & \boldsymbol{g}(t_f)^T \\ \dot{\boldsymbol{g}}(t_f)^T & \boldsymbol{0} \end{bmatrix} \tag{31}$$

and the initial and final state vectors $\boldsymbol{b}_i$ and $\boldsymbol{b}_f$ take the form

$$\boldsymbol{b}_i = \begin{bmatrix} x_i \\ y_i \\ \dot{x}_i \end{bmatrix} \quad \text{and } \boldsymbol{b}_f = \begin{bmatrix} x_f \\ y_f \\ \dot{x}_f \end{bmatrix} \tag{32}$$

Moreover, by employing the expansion of Eq. (26), the dynamic constraint $\phi(y, D^r y, \dot{x}) = 0$ of Eq. (24), which needs to be satisfied for all $t \in [t_i, t_f]$, is approximated by $\bar{\phi}(\boldsymbol{c}, t) = \phi(\bar{y}, D^r \bar{y}, \dot{\bar{x}}) = 0$, and is equivalently expressed as

$$\xi(\boldsymbol{c}) := \int_{t_i}^{t_f} [\bar{\phi}(\boldsymbol{c}, t)]^2 \mathrm{d}t = 0 \tag{33}$$

Next, taking into account both the constraint of Eq. (30) and the constraint of Eq. (33), the constrained variational problem in

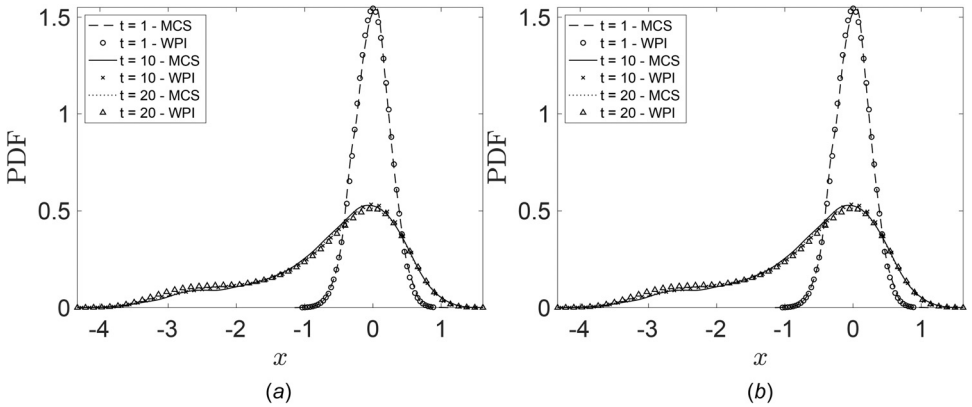

Fig. 3 Marginal response PDFs of a nonlinear energy harvester with $\zeta = 0.1$, $\kappa = 0.65$, $\alpha = 0.8$, $\delta = 0.2$, $S_0 = 0.05$, and fractional derivative order $r = 0.75$ for three (nondimensional) time instants $t = 1$, $t = 10$, and $t = 20$. Comparison with MCS data (10,000 realizations). (*a*) Displacement x and (*b*) electrical quantity y.

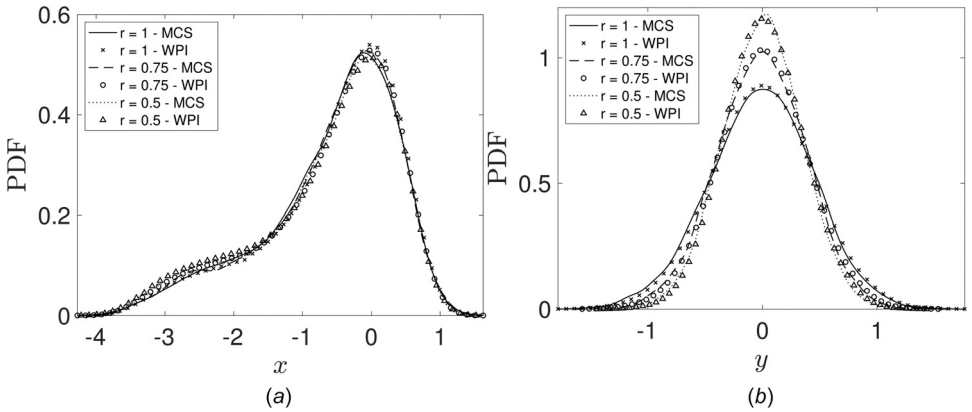

Fig. 4 Stationary marginal response PDFs of a nonlinear energy harvester with $\zeta = 0.1$, $\kappa = 0.65$, $\alpha = 0.8$, $\delta = 0.2$, and $S_0 = 0.05$ for various values of the fractional derivative order $r = 1$, $r = 0.75$, and $r = 0.5$. Comparison with MCS data (10,000 realizations). (*a*) Displacement x and (*b*) electrical quantity y.

Eqs. (24) and (25) is reformulated as a constrained optimization problem in the form

$$J_f^* = \min_{\boldsymbol{c}\in\mathbb{R}^{nL}} J(\boldsymbol{c}) \quad \text{subject to} \quad \xi(\boldsymbol{c}) = 0 \quad \begin{bmatrix} \boldsymbol{A}_i \\ \boldsymbol{A}_f \end{bmatrix} \boldsymbol{c} = \begin{bmatrix} \boldsymbol{b}_i \\ \boldsymbol{b}_f \end{bmatrix} \tag{34}$$

Further, according to Eq. (20) and assuming fixed initial conditions $\boldsymbol{b}_i$ at t_i (e.g., system initially at rest), a specific point of the response transition PDF corresponding to final state $\boldsymbol{b}_f$ at t_f is determined as

$$\bar{p}(\boldsymbol{b}_f, t_f|\boldsymbol{b}_i, t_i) = C\exp(-J_f^*) \tag{35}$$

where C is a normalization constant. Obviously, choosing a sufficiently large final time instant t_f Eq. (35) converges to the stationary joint response PDF $p_s(\boldsymbol{b}_f) = \bar{p}(\boldsymbol{b}_f, t_f|\boldsymbol{b}_i, t_i)$. The optimization problem of Eq. (34), which has both linear and nonlinear equality constraints, is solved in the following examples by a standard interior point method presented in Refs. [48] and [49].

5 Numerical Examples

To demonstrate the reliability of the proposed technique for analyzing and optimizing energy harvesting systems, a monostable asymmetric nonlinear harvester ($0 \le \lambda \le 2\sqrt{\delta}$, $\delta \ge 0$) with a fractional derivative term described by Eq. (3) is considered in this section. First, to demonstrate the accuracy of the adapted WPI technique described in Sec. 4, the stationary marginal response PDFs are determined and compared with pertinent MCS data. Next, optimal energy harvester designs are obtained by employing the aforementioned WPI technique in conjunction with Eq. (5) as the objective function of a global optimization algorithm, constrained via a prescribed probability of failure (see Eqs. (7) and (12)).

5.1 Energy Harvester Stochastic Response Analysis. The nonlinear energy harvester with monostable asymmetric potential (see Eq. (3)) and parameters $\zeta = 0.1$, $\kappa = 0.65$, $\alpha = 0.8$, $\delta = 0.2$, and $S_0 = 0.05$ is considered next. The stationary marginal response PDFs $p_s(x)$ and $p_s(y)$ for fractional derivative order $r = 0.75$ and for three (nondimensional) time instants $t = 1$, $t = 10$, and $t = 20$ are shown in Fig. 3 and compared with pertinent MCS data. It is observed that the system has practically reached stationarity for $t = 10$. Clearly, the WPI technique exhibits a high degree of accuracy in determining the stochastic response of the nonlinear harvester, even for the challenging case of the strongly non-Gaussian and asymmetric displacement PDF $p_s(x)$.

Moreover, the stationary marginal response PDFs determined by the WPI technique for fractional derivative order r values 1, 0.75, and 0.5 are shown in Fig. 4 and compared with pertinent MCS data. The WPI technique exhibits a high degree of accuracy

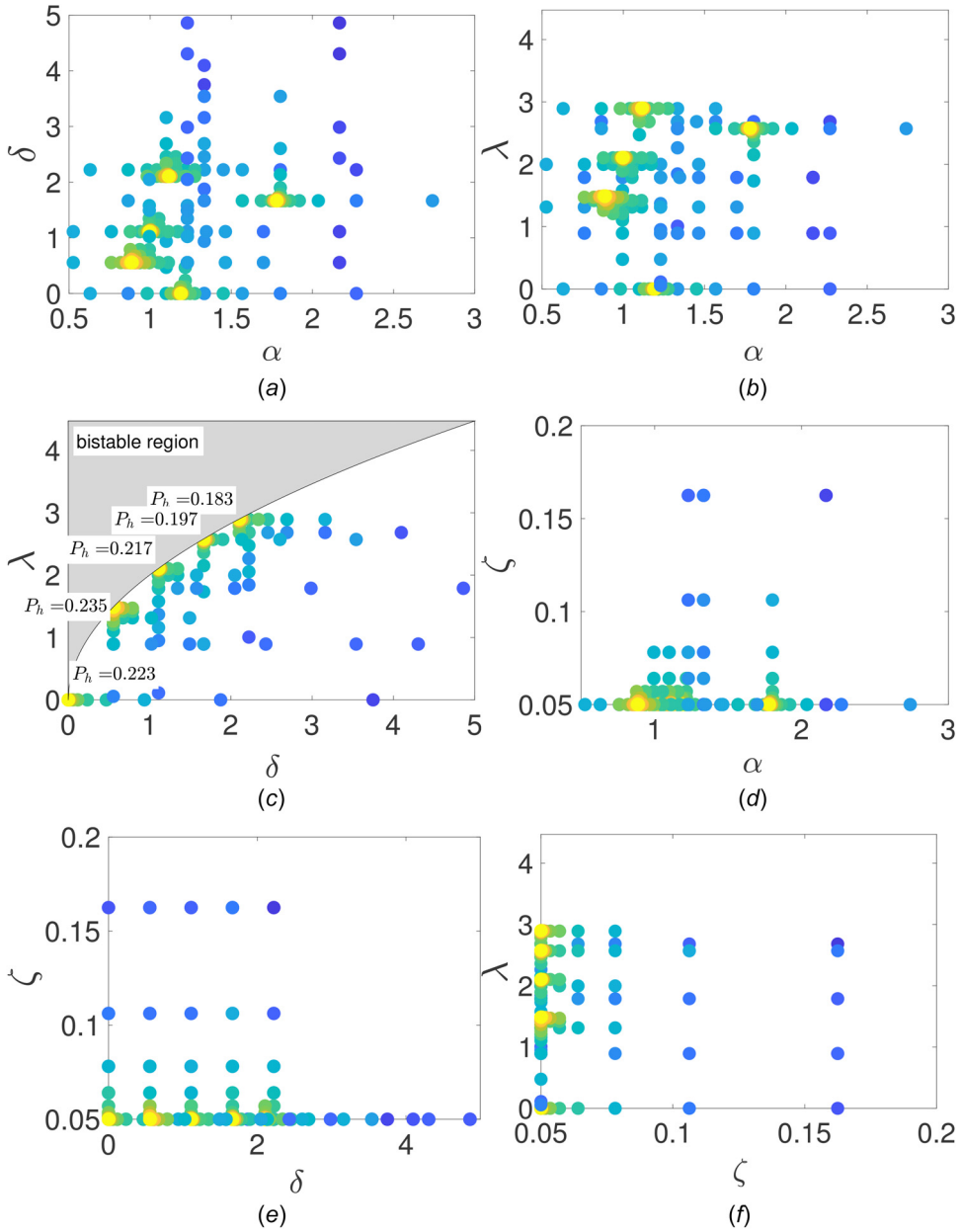

Fig. 5 Two-dimensional projections of computed points (color varies with iteration count). Optimization by GPS algorithm with $z = [\alpha, \delta, \zeta, \lambda]^T \in [0.5, 3] \times [0, 5] \times [0.05, 0.2] \times [0, 2\sqrt{\delta}]$, $\kappa = 0.65$, $r = 1$, and unconstrained probability of failure ($L_b = \infty$). (*a*) $L_b = \infty$, α–δ plane, (*b*) $L_b = \infty$, α–λ plane, (*c*) $L_b = \infty$, δ–λ plane, (*d*) $L_b = \infty$, α–ζ plane, (*e*) $L_b = \infty$, δ–ζ plane, and (*f*) $L_b = \infty$, ζ–λ plane.

in determining the response PDFs, for all considered values of the fractional derivative order. Obviously, the impact of the fractional derivative order is larger on the electrical quantity y (as compared to x), since the fractional derivative in Eq. (1*b*) operates directly on y.

5.2 Energy Harvester Design Optimization. In this section, the results of a four-parameter (α, δ, ζ, λ) and a two-parameter (α, δ) harvester design optimization problems, both with and without constraints related to probability of failure, are presented and discussed. In both cases, the optimal locations δx^* are provided as well according to the formulation in Sec. 2.2.

5.2.1 Four-Parameter Design Optimization. The general four-parameter optimization problem is considered herein with $z = [\alpha, \delta, \zeta, \lambda]^T \in [0.5, 3] \times [0, 5] \times [0.05, 0.2] \times [0, 2\sqrt{\delta}]$ and fractional derivative order $r = 1$. The GPS algorithm [38] is utilized for the solution of the optimization problem of Eq. (7) with constrained P_f defined in Eq. (12), whereas the unconstrained case is studied as well by setting $L_b \to \infty$.

Since the GPS algorithm is not guaranteed to converge to the global optimum, five optimization chains are considered, i.e., five independent optimization runs starting from different initial points, to increase the probability of converging to the global optimum. These five initial points are chosen based on the rationale described in the following. First, the four-dimensional input space is discretized into a coarse grid of 961 points and the marginal PDFs of x and y corresponding to each grid point are obtained by utilizing the WPI technique presented in Sec. 4.2. Next, the points violating the condition $\lambda \leq 2\sqrt{\delta}$, and/or leading to failure with respect to the specific box size parameter L_b and probability threshold ϵ, are discarded. The 30 feasible points yielding the highest energy output P_h are identified and the one corresponding to the highest overall P_h value is selected as the first initial point.

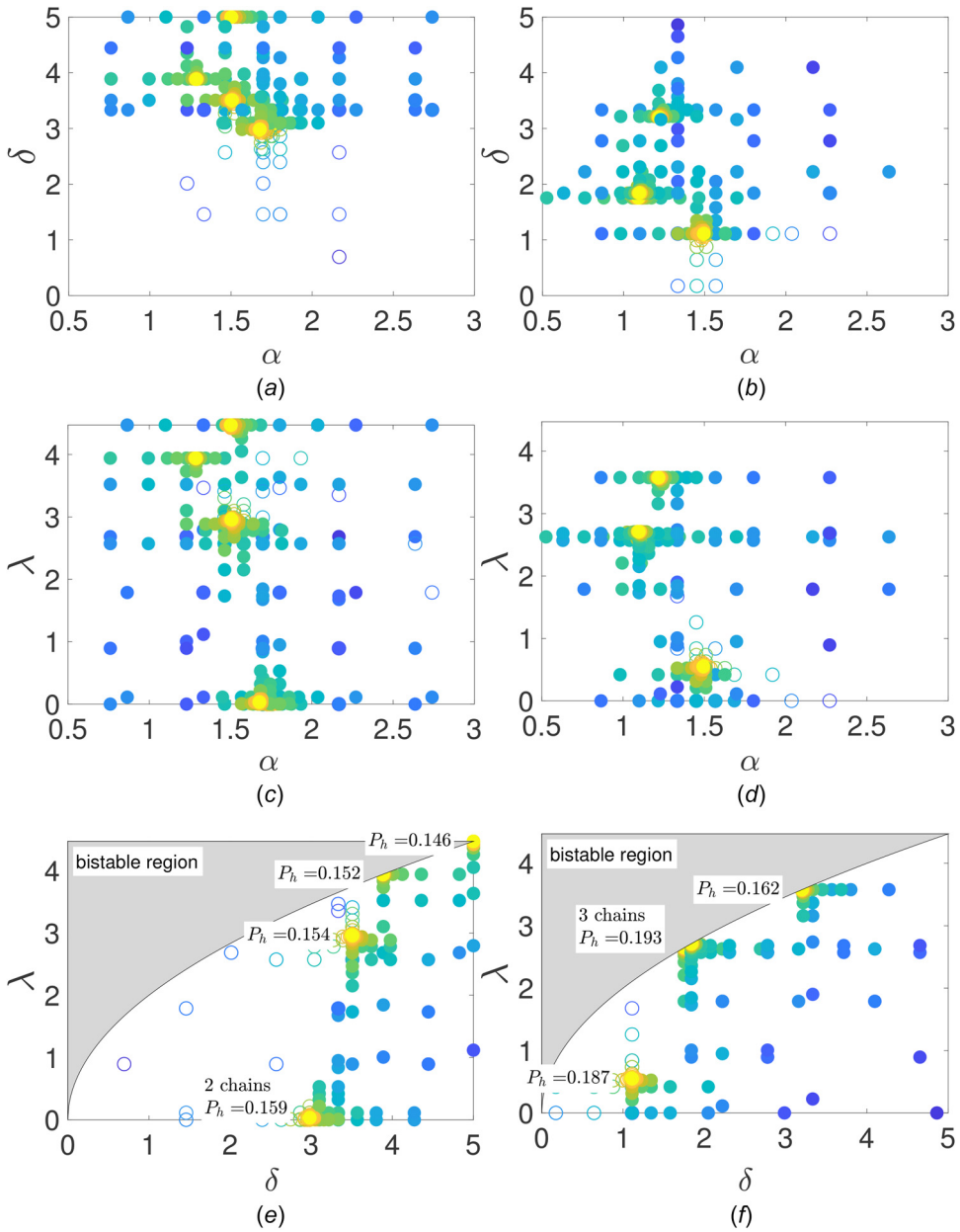

Fig. 6 Two-dimensional projections of computed points (color varies with iteration count and unfilled circles correspond to probabilities of failure larger than ϵ). Optimization by GPS algorithm with $z = [\alpha, \delta, \zeta, \lambda]^T \in [0.5, 3] \times [0, 5] \times [0.05, 0.2] \times [0, 2\sqrt{\delta}]$, $\kappa = 0.65$, $r = 1$, and constrained probability of failure with L_b equal to 2.4 ((*a*), (*c*), and (*e*)) and 3 ((*b*), (*d*), and (*f*)) and $\epsilon = 10^{-3}$. (*a*) $L_b = 2.4$, α–δ plane, (*b*) $L_b = 3$, α–δ plane, (*c*) $L_b = 2.4$, α–λ plane, (*d*) $L_b = 3$, α–λ plane, (*e*) $L_b = 2.4$, δ–λ plane, and (*f*) $L_b = 3$, δ–λ plane.

Table 1 Summary of optimal energy harvester designs for $z = [\alpha, \delta, \zeta, \lambda]^T \in [0.5, 3] \times [0, 5] \times [0.05, 0.2] \times [0, 2\sqrt{\delta}]$, $\kappa = 0.65$, $r = 1$, and different box sizes L_b

	Optimal design						
Box size L_b	α^*	δ^*	ζ^*	λ^*	δx^*	Average power P_h	Probability of failure P_f
2.3	1.761	3.573	0.05	0.000	0.000	0.1514	0.000999
2.4	1.678	2.982	0.05	0.033	0.005	0.1593	0.000997
2.5	1.678	2.510	0.05	0.013	0.002	0.1635	0.000994
2.6	1.640	2.112	0.05	0.003	0.001	0.1701	0.000999
2.7	1.610	1.810	0.05	0.105	0.025	0.1736	0.000936
2.8	1.557	1.503	0.05	0.004	0.001	0.1807	0.000993
2.9	1.115	1.973	0.05	2.809	0.565	0.1864	0.000780
3.0	1.090	1.753	0.05	2.648	0.557	0.1926	0.000727
∞	0.887	0.556	0.05	1.491	—	0.2349	0.000000

Unconstrained ($L_b = \infty$) and constrained probability of failure with $\epsilon = 10^{-3}$.

Table 2 Summary of optimal energy harvester designs for $z=[\alpha,\delta]^T \in [0.5,3]\times[0,5]$, $\lambda=0$, $\zeta=0.05$, $\kappa=0.65$, $r=1$, and different box sizes L_b

Box size	Optimal design			Average power	Probability of failure
L_b	α^*	δ^*	δx^*	P_h	P_f
2.3	1.765	3.574	0.000	0.1516	0.001000
2.4	1.750	3.008	0.000	0.1578	0.000971
2.5	1.672	2.578	0.000	0.1624	0.000879
2.6	1.638	2.130	0.000	0.1680	0.000962
2.7	1.589	1.782	0.000	0.1738	0.000991
2.8	1.560	1.509	0.000	0.1787	0.000982
2.9	1.574	1.289	0.000	0.1837	0.000969
3.0	1.480	1.082	0.000	0.1906	0.000995
∞	1.190	0.000	—	0.2231	0.000000

Unconstrained ($L_b=\infty$) and constrained probability of failure with $\epsilon=10^{-3}$.

Table 3 Summary of optimal energy harvester designs for $z=[\alpha,\delta]^T \in [0.5,3]\times[0,5]$, $\lambda=2\sqrt{\delta}$, $\zeta=0.05$, $\kappa=0.65$, $r=1$, and different box sizes L_b

Box size	Optimal design			Average power	Probability of failure
L_b	α^*	δ^*	δx^*	P_h	P_f
2.3	1.325	4.407	0.442	0.1465	0.000997
2.4	1.284	3.801	0.488	0.1533	0.000999
2.5	1.252	3.259	0.516	0.1607	0.000905
2.6	1.188	2.823	0.537	0.1677	0.000996
2.7	1.195	2.477	0.550	0.1746	0.000989
2.8	1.130	2.178	0.558	0.1817	0.000972
2.9	1.103	1.917	0.559	0.1898	0.000992
3.0	1.086	1.659	0.572	0.1952	0.000963
∞	0.890	0.459	—	0.2373	0.000000

Unconstrained ($L_b=\infty$) and constrained probability of failure with $\epsilon=10^{-3}$.

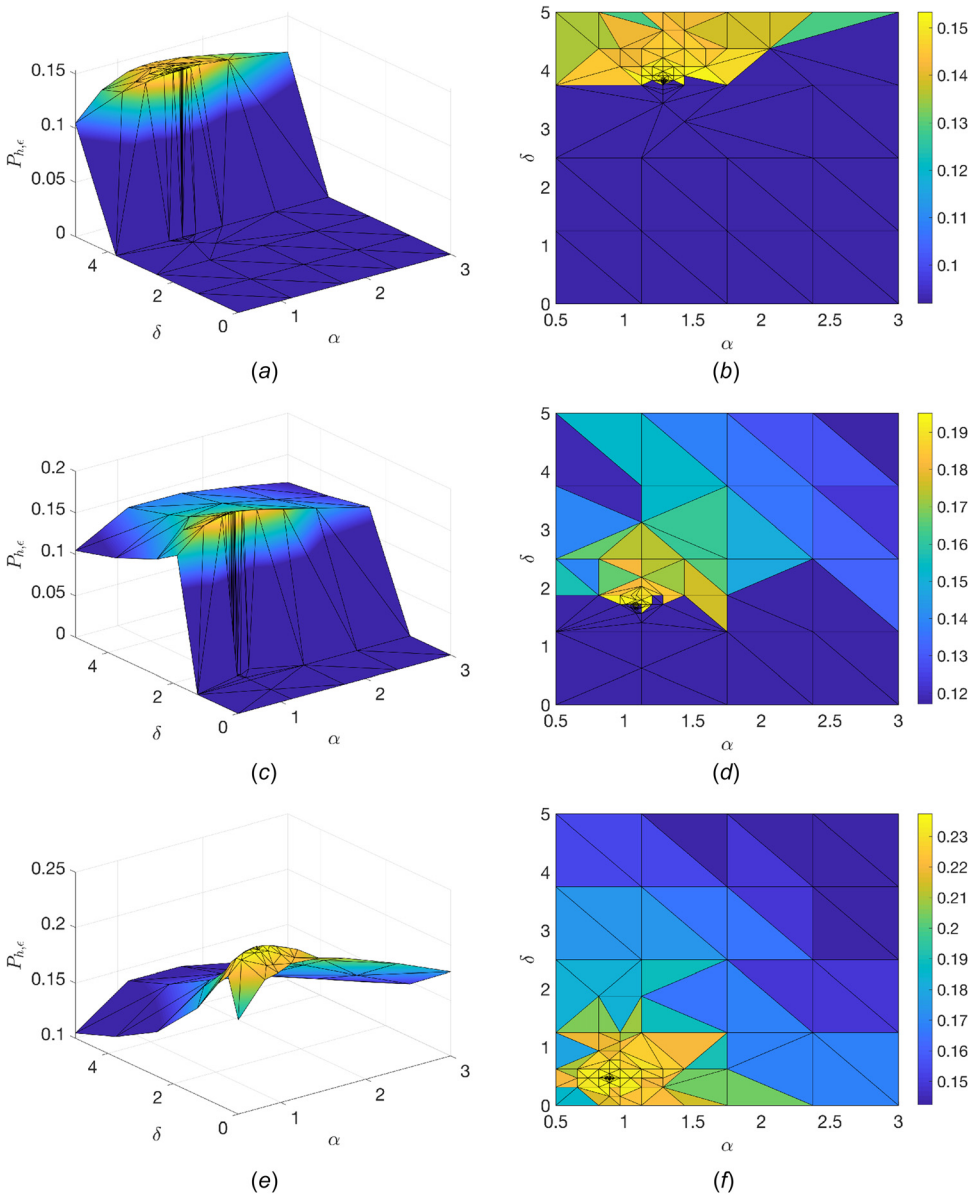

Fig. 7 Stationary mean harvested power P_h. Optimization by GPS algorithm with $z=[\alpha,\delta]^T \in [0.5,3]\times[0,5]$, $\lambda=2\sqrt{\delta}$, $\zeta=0.05$, $\kappa=0.65$, $r=1$. ((*a*), (*c*), and (*e*)) Three-dimensional (3D) surface plots with gradient coloring. ((*b*), (*d*), and (*f*)) Overview plots with flat coloring. (*a*) Three-dimensional plot—$L_b=2.4$, (*b*) overview plot—$L_b=2.4$, (*c*) 3D plot—$L_b=3$, (*d*) overview plot—$L_b=3$, (*e*) 3D plot—$L_b=\infty$, and (*f*) overview plot—$L_b=\infty$.

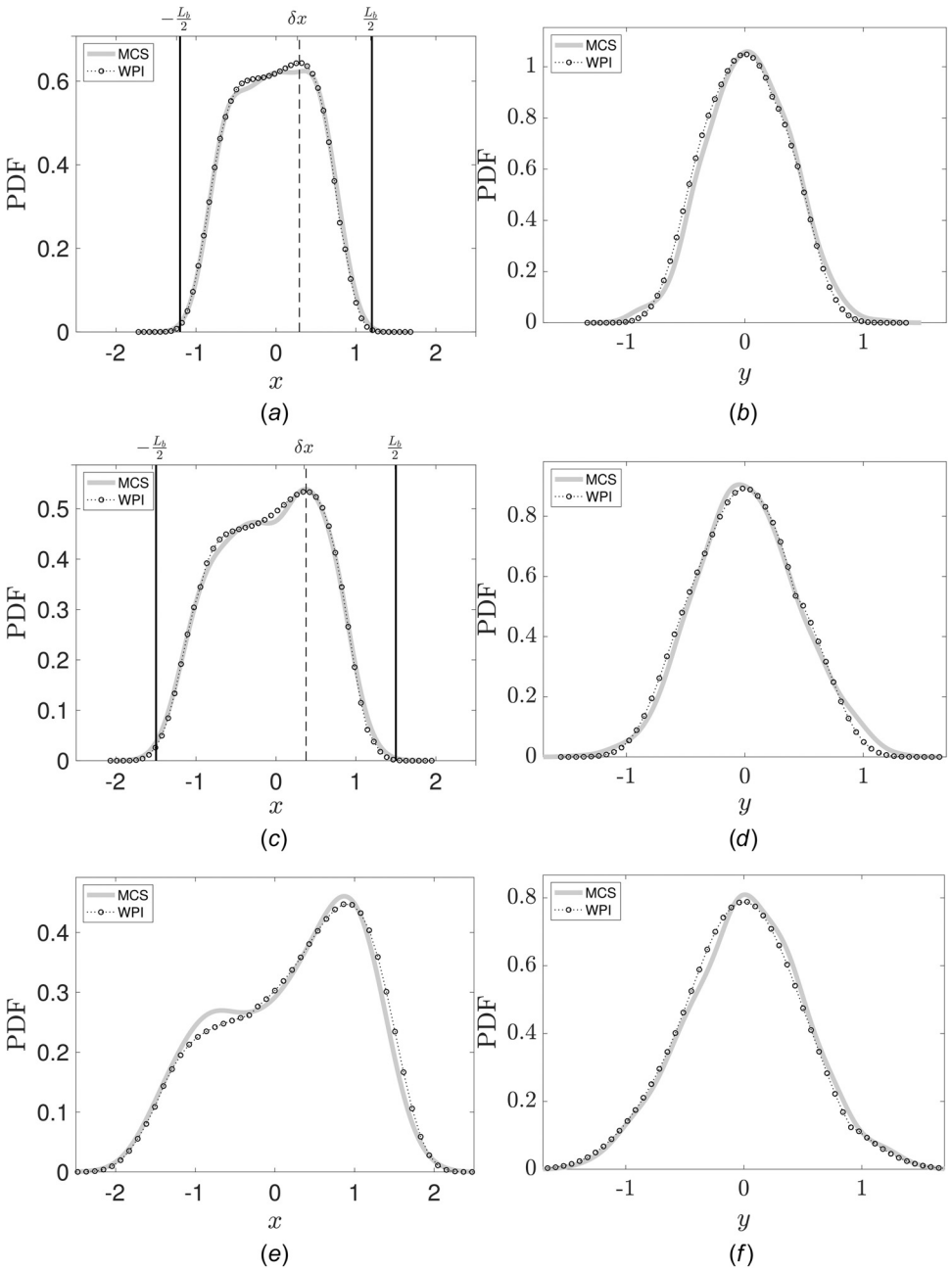

Fig. 8 Response PDFs of three optimal designs corresponding to box size parameter L_b values of 2.4, 3, and ∞; see second, eighth, and ninth rows of Table 3, respectively, for optimal design parameters (α^*, δ^*), shift parameter δx, mean harvested power P_h and probability of failure P_f. (*a*) Displacement *x*—$L_b = 2.4$, (*b*) electrical quantity *y*—$L_b = 2.4$, (*c*) displacement *x*—$L_b = 3$, (*d*) electrical quantity *y*—$L_b = 3$, (*e*) displacement *x*—$L_b = \infty$, and (*f*) electrical quantity *y*—$L_b = \infty$.

Further, the remaining four initial points for each optimization chain are chosen among the rest of the 29 points as the ones exhibiting the largest sum of distances with respect to the other points. Clearly, this procedure selects initial points with the following desirable properties: (a) they are feasible; (b) they are located in regions corresponding to high energy output; and (c) they are reasonably dispersed over these high output regions.

The results of the five optimization chains for the unconstrained probability of failure case ($L_b \to \infty$) are plotted in Fig. 5 as projections on two-dimensional planes, where the color of the circles varies with the iteration number (starting from dark blue and converging to yellow). This representation provides a crude illustration of the optimization solution path in the four-dimensional space. It is seen that the five chains converged to different points characterized by different mean harvester power outputs, and that all converged points are located on the bistability limit $\lambda = 2\sqrt{\delta}$. Moreover, the optimal parameter ζ^* reaches its lower bound of 0.05 (see Figs. 5(*d*)–5(*f*)). This is anticipated as a mechanical system with low damping leads to higher amplitude vibrations, and thus, to higher harvested power.

However, in many practical implementations, space limitations dictate constraints on the vibration amplitude, such as the one described by Eqs. (7)–(12). In this regard, and focusing on the constrained optimization problem of Eqs. (7)–(12) with $\epsilon = 10^{-3}$, the results of the five optimization chains are shown in Fig. 6 for two design examples with $L_b = 2.4$ (Figs. 6(*a*), 6(*c*), and 6(*e*)) and $L_b = 3$ (Figs. 6(*b*), 6(*d*), and 6(*f*)). In these examples, some chains converge to designs, which do not correspond to the bistability

Table 4 Summary of optimal energy harvester designs for $z=[\alpha,\delta]^T \in [0.5,3]\times[0,5]$, $\lambda=2\sqrt{\delta}$, $\zeta=0.05$, $\kappa=0.65$, $r=0.75$, and different box sizes L_b

Box size	Optimal design			Average power	Probability of failure
L_b	α^*	δ^*	δx^*	P_h	P_f
2.3	1.408	4.531	0.429	0.1235	0.000917
2.4	1.359	3.906	0.476	0.1280	0.000907
2.5	1.398	3.350	0.509	0.1331	0.000983
2.6	1.555	2.969	0.521	0.1377	0.000941
2.7	1.440	2.617	0.540	0.1419	0.000832
2.8	1.438	2.266	0.552	0.1471	0.000953
2.9	1.379	1.992	0.559	0.1505	0.000881
3.0	1.474	1.783	0.553	0.1593	0.000916
∞	1.047	0.625	—	0.1767	0.000000

Unconstrained ($L_b=\infty$) and constrained probability of failure with $\epsilon=10^{-3}$.

Table 5 Summary of optimal energy harvester designs for $z=[\alpha,\delta]^T \in [0.5,3]\times[0,5]$, $\lambda=2\sqrt{\delta}$, $\zeta=0.05$, $\kappa=0.65$, $r=0.50$, and different box sizes L_b

Box size	Optimal design			Average power	Probability of failure
L_b	α^*	δ^*	δx^*	P_h	P_f
2.3	1.398	4.492	0.433	0.1102	0.000920
2.4	1.438	3.866	0.478	0.1136	0.000975
2.5	1.357	3.330	0.513	0.1177	0.000942
2.6	1.320	2.930	0.533	0.1213	0.000867
2.7	1.276	2.490	0.553	0.1252	0.000989
2.8	1.342	2.224	0.559	0.1288	0.000983
2.9	1.474	2.012	0.556	0.1317	0.000981
3.0	1.408	1.787	0.556	0.1369	0.000901
∞	1.875	1.000	—	0.1569	0.000000

Unconstrained ($L_b=\infty$) and constrained probability of failure with $\epsilon=10^{-3}$.

limit ($\lambda=2\sqrt{\delta}$). In fact, it can be seen in Fig. 6(*e*) that for a relatively "tight" box with $L_b=2.4$, the global optimum found yields a symmetric harvester, i.e., $\lambda\approx 0$. This trend is evident in Table 1, which summarizes the optimal (among the five chains) results, for various examples with increasing L_b, including the unconstrained case ($L_b=\infty$). Indeed, note that for $L_b<2.9$, the optimal harvester is approximately symmetric ($\lambda\approx 0$), whereas for $L_b\geq 2.9$ the constraint on the probability of failure becomes less severe and asymmetric designs appear to yield higher power output. In fact, these asymmetric designs tend to converge to the bistability limit with $\lambda=2\sqrt{\delta}$. Moreover, as the available space L_b decreases, the parameter δ^* is increased to provide additional stiffness and restrict the oscillator within the gradually tighter bounds.

5.2.2 Two-Parameter Design Optimization. According to the results of the four-parameter design optimization examples presented in Table 1, ζ^* always takes its lower bound value, while λ^* converges either to its lower allowable value of 0 or to the bistability limit $2\sqrt{\delta}$. Motivated by the above observations, a two-parameter design optimization is pursued in this section aiming at enhanced computational efficiency and more robust convergence behavior. Specifically, z in Eq. (7) becomes $z=[\alpha,\delta]^T\in[0.5,3]\times[0,5]$ with $\zeta=0.05$, $\kappa=0.65$. Two distinct values of lambda are considered in the examples, i.e., $\lambda=0$ and $\lambda=2\sqrt{\delta}$. Notably, employing a similar approach as in Sec. 5.2.1, all five optimization chains applied for a given set of fixed parameters converged to the same optimal point. Clearly, this indicates that the two-parameter optimization exhibits a more robust convergence behavior than its four-parameter counterpart. For various values of the box size parameter L_b the converged optimal points are presented in Table 2 for $\lambda=0$ and in Table 3 for $\lambda=2\sqrt{\delta}$. Moreover, Fig. 7 depicts the points accessed by the five optimization chains for $\lambda=2\sqrt{\delta}$, and box size parameter L_b equal to 2.4, 3, and ∞.

It is seen in Tables 2 and 3 that, similarly to the four-parameter optimization of Sec. 5.2.1, for relatively small box sizes L_b the symmetric design ($\lambda=0$, Table 2) outperforms the asymmetric design ($\lambda=2\sqrt{\delta}$, Table 3), whereas as L_b increases, asymmetry leads to higher energy output, even for the unconstrained case ($L_b=\infty$). Further, the theoretically supported fact (e.g., Refs. [31] and [33–35]), that the linear design, i.e., $\delta=0$, is optimal among symmetric ($\lambda=0$) and unconstrained ($L_b\to\infty$) harvesters, is further corroborated by the herein analysis; see last row of Table 2. In contrast, it appears that the introduction of asymmetric nonlinearities, i.e., $\delta>0$ and $\lambda=2\sqrt{\delta}$ yields designs that outperform significantly the linear design in terms of energy output; this is also in agreement with conclusions drawn in Refs. [20,21], and [36] based on relevant numerical studies. Moreover, considering the shape of the surface plots in Fig. 7, and that all five chains converged to the same point, indicates the existence of a single (global) optimum for the two-parameter optimization case.

Next, attention is directed to three indicative optimal harvesters in Table 3 with L_b values of 2.4, 3, and ∞. The corresponding stationary marginal response PDFs $p_s(x)$ and $p_s(y)$ are obtained by employing the herein adapted WPI technique. These are plotted in Fig. 8 and compared with MCS data. Besides the relatively high degree of accuracy exhibited by the WPI technique, it is seen in Figs. 8(*a*) and 8(*c*) that the optimal shape of $p_s(x)$ tends toward a rectangular form. This is anticipated, since this particular shape of $p_s(x)$ leads, in general, to low probability of failure. Also, it corresponds to a relatively higher variance of x, and therefore (see Eq. (1*a*)), to a higher variance of y as well, i.e., higher energy output (see Eq. (5)).

5.2.3 Two-Parameter Design Optimization for Various Fractional Derivative Order Values. In this subsection, the two-parameter design optimization problem of Sec. 5.2.2 is considered for harvesters with $\lambda=2\sqrt{\delta}$ and with two distinct fractional derivative order values, i.e., $r=0.75$ and $r=0.50$. The results are summarized in Table 4 for $r=0.75$ and in Table 5 for $r=0.50$. The conclusions are similar to Sec. 5.2.2 (see Table 3), while it is evident that the energy output decreases for decreasing fractional derivative order r as shown in Sec. 5.1 (see Fig. 4(*b*)).

6 Concluding Remarks

In this paper, a WPI-based methodology has been developed for stochastic response determination and reliability-based design optimization of a class of energy harvesters exhibiting asymmetric nonlinearities and endowed with fractional derivative elements. To this aim, first, the WPI stochastic dynamics solution technique has been adapted and enhanced for addressing the peculiarities of the coupled electromechanical governing equations; that is, the presence of a singular diffusion matrix and of a fractional derivative term associated with the capacitance. Specifically, following a variational formulation for the WPI, and interpreting the electrical equation as a dynamic constraint to a stochastically excited underdetermined SDE, has led to a Rayleigh–Ritz direct minimization problem for determining the system joint response PDF.

Next, the WPI technique has been coupled with a gradient-free optimization algorithm for determining the harvester optimal parameters subject to constraints relating to probabilities of failure. In fact, a rather pragmatic failure definition has been proposed herein suitable for harvester configurations subject to space limitations. Notably, this definition also leads to obtaining the optimal position of the harvester within a predefined operational width (box); thus, the potentially limited available space is fully exploited. Several numerical examples have been considered

demonstrating the satisfactory performance of the methodology. Comparisons with pertinent MCS data have been included as well showing a relatively high accuracy degree.

Further, it is worth highlighting the following observations based on the numerical analyses: (a) among the symmetric monostable nonlinear harvesters with cubic nonlinearity, the linear design is shown to be the optimum (see last row of Table 2 and also Refs. [31] and [33–35]); (b) the presence of asymmetry, i.e., quadratic nonlinearities in addition to the cubic nonlinear term, leads to nonlinear designs that outperform the linear harvester (see last rows of both Tables 2 and 3 and also Refs. [21] and [36]); and (c) in the four-parameter design optimization of Sec. 5.2.1, most chains converge to points where the asymmetry parameter takes values on the bistability limit $\lambda = 2\sqrt{\delta}$ (see Figs. 5 and 6). Note that this is the maximum allowed value since only monostable harvesters have been considered herein. This is a strong indication that the mean harvested power (i.e., objective function) exhibits larger values for $\lambda > 2\sqrt{\delta}$. In other words, this finding supports results in the literature indicating that bistable harvesters outperform, in general, monostable harvesters (e.g., Refs. [5,22,30,32,33,50], and [51]).

Acknowledgment

I. A. Kougioumtzoglou gratefully acknowledges the support through his CAREER award by the CMMI Division of the National Science Foundation, U.S. (Award No. 1748537).

References

[1] Sodano, H. A., Inman, D. J., and Park, G., 2004, "A Review of Power Harvesting From Vibration Using Piezoelectric Materials," Shock Vib. Dig., **36**(3), pp. 197–206.
[2] Sodano, H. A., Inman, D. J., and Park, G., 2005, "Generation and Storage of Electricity From Power Harvesting Devices," J. Intell. Mater. Syst. Struct., **16**(1), pp. 67–75.
[3] Wu, W.-J., Chen, Y.-Y., Lee, B.-S., He, J.-J., and Peng, Y.-T., 2006, "Tunable Resonant Frequency Power Harvesting Devices," Smart Structures and Materials 2006: Damping and Isolation, San Diego, CA, p. 61690A.
[4] Soliman, M., Abdel-Rahman, E., El-Saadany, E., and Mansour, R., 2008, "A Wideband Vibration-Based Energy Harvester," J. Micromech. Microeng., **18**(11), p. 115021.
[5] Daqaq, M. F., Masana, R., Erturk, A., and Quinn, D. D., 2014, "On the Role of Nonlinearities in Vibratory Energy Harvesting: A Critical Review and Discussion," ASME Appl. Mech. Rev., **66**(4), p. 040801.
[6] Gammaitoni, L., Neri, I., and Vocca, H., 2009, "Nonlinear Oscillators for Vibration Energy Harvesting," Appl. Phys. Lett., **94**(16), p. 164102.
[7] Adhikari, S., Friswell, M., and Inman, D., 2009, "Piezoelectric Energy Harvesting From Broadband Random Vibrations," Smart Mater. Struct., **18**(11), p. 115005.
[8] Barton, D. A., Burrow, S. G., and Clare, L. R., 2010, "Energy Harvesting From Vibrations With a Nonlinear Oscillator," ASME J. Vib. Acoust., **132**(2), p. 021009.
[9] Daqaq, M. F., 2011, "Transduction of a Bistable Inductive Generator Driven by White and Exponentially Correlated Gaussian Noise," J. Sound Vib., **330**(11), pp. 2554–2564.
[10] Yoon, H., and Youn, B. D., 2014, "Stochastic Quantification of the Electric Power Generated by a Piezoelectric Energy Harvester Using a Time–Frequency Analysis Under Non-Stationary Random Vibrations," Smart Mater. Struct., **23**(4), p. 045035.
[11] Freeborn, T. J., Maundy, B., and Elwakil, A. S., 2015, "Fractional-Order Models of Supercapacitors, Batteries and Fuel Cells: A Survey," Mater. Renewable Sustainable Energy, **4**(3), p. 9.
[12] Allagui, A., Freeborn, T. J., Elwakil, A. S., Fouda, M. E., Maundy, B. J., Radwan, A. G., Said, Z., and Abdelkareem, M. A., 2018, "Review of Fractional-Order Electrical Characterization of Supercapacitors," J. Power Sources, **400**, pp. 457–467.
[13] Ngueuteu, G. M., and Woafo, P., 2012, "Dynamics and Synchronization Analysis of Coupled Fractional-Order Nonlinear Electromechanical Systems," Mech. Res. Commun., **46**, pp. 20–25.
[14] Kwuimy, C. K., Litak, G., and Nataraj, C., 2015, "Nonlinear Analysis of Energy Harvesting Systems With Fractional Order Physical Properties," Nonlinear Dyn., **80**(1–2), pp. 491–501.
[15] Erturk, A., and Inman, D. J., 2011, *Piezoelectric Energy Harvesting*, Wiley, Hoboken, NJ.
[16] Litak, G., Friswell, M., and Adhikari, S., 2010, "Magnetopiezoelastic Energy Harvesting Driven by Random Excitations," Appl. Phys. Lett., **96**(21), p. 214103.
[17] Daqaq, M. F., 2010, "Response of Uni-Modal Duffing-Type Harvesters to Random Forced Excitations," J. Sound Vib., **329**(18), pp. 3621–3631.
[18] Green, P., Worden, K., Atallah, K., and Sims, N., 2012, "The Benefits of Duffing-Type Nonlinearities and Electrical Optimisation of a Mono-Stable Energy Harvester Under White Gaussian Excitations," J. Sound Vib., **331**(20), pp. 4504–4517.
[19] Adhikari, S., Friswell, M., Litak, G., and Khodaparast, H. H., 2016, "Design and Analysis of Vibration Energy Harvesters Based on Peak Response Statistics," Smart Mater. Struct., **25**(6), p. 065009.
[20] Petromichelakis, I., Psaros, A. F., and Kougioumtzoglou, I. A., 2018, "Stochastic Response Determination and Optimization of a Class of Nonlinear Electromechanical Energy Harvesters: A Wiener Path Integral Approach," Probab. Eng. Mech., **53**, pp. 116–125.
[21] He, Q., and Daqaq, M. F., 2016, "Electric Load Optimization of a Nonlinear Mono-Stable Duffing Harvester Excited by White Noise," Meccanica, **51**(5), pp. 1027–1039.
[22] Ali, S., Adhikari, S., Friswell, M., and Narayanan, S., 2011, "The Analysis of Piezomagnetoelastic Energy Harvesters Under Broadband Random Excitations," J. Appl. Phys., **109**(7), p. 074904.
[23] Kougioumtzoglou, I., and Spanos, P., 2012, "An Analytical Wiener Path Integral Technique for Non-Stationary Response Determination of Nonlinear Oscillators," Probab. Eng. Mech., **28**, pp. 125–131.
[24] Kougioumtzoglou, I. A., and Spanos, P. D., 2014, "Nonstationary Stochastic Response Determination of Nonlinear Systems: A Wiener Path Integral Formalism," J. Eng. Mech., **140**(9), p. 04014064.
[25] Kougioumtzoglou, I. A., Di Matteo, A., Spanos, P. D., Pirrotta, A., and Di Paola, M., 2015, "An Efficient Wiener Path Integral Technique Formulation for Stochastic Response Determination of Nonlinear MDOF Systems," ASME J. Appl. Mech., **82**(10), p. 101005.
[26] Kougioumtzoglou, I. A., 2017, "A Wiener Path Integral Solution Treatment and Effective Material Properties of a Class of One-Dimensional Stochastic Mechanics Problems," J. Eng. Mech., **143**(6), p. 04017014.
[27] Di Matteo, A., Kougioumtzoglou, I. A., Pirrotta, A., Spanos, P. D., and Di Paola, M., 2014, "Stochastic Response Determination of Nonlinear Oscillators With Fractional Derivatives Elements Via the Wiener Path Integral," Probab. Eng. Mech., **38**, pp. 127–135.
[28] Cottone, F., Vocca, H., and Gammaitoni, L., 2009, "Nonlinear Energy Harvesting," Phys. Rev. Lett., **102**(8), p. 080601.
[29] Nguyen, S. D., and Halvorsen, E., 2011, "Nonlinear Springs for Bandwidth-Tolerant Vibration Energy Harvesting," J. Microelectromech. Syst., **20**(6), pp. 1225–1227.
[30] Daqaq, M. F., 2012, "On Intentional Introduction of Stiffness Nonlinearities for Energy Harvesting Under White Gaussian Excitations," Nonlinear Dyn., **69**(3), pp. 1063–1079.
[31] Halvorsen, E., 2013, "Fundamental Issues in Nonlinear Wideband-Vibration Energy Harvesting," Phys. Rev. E, **87**(4), p. 042129.
[32] Harne, R., and Wang, K., 2013, "A Review of the Recent Research on Vibration Energy Harvesting Via Bistable Systems," Smart Mater. Struct., **22**(2), p. 023001.
[33] Joo, H. K., and Sapsis, T. P., 2014, "Performance Measures for Single-Degree-of-Freedom Energy Harvesters Under Stochastic Excitation," J. Sound Vib., **333**(19), pp. 4695–4710.
[34] Langley, R., 2014, "A General Mass Law for Broadband Energy Harvesting," J. Sound Vib., **333**(3), pp. 927–936.
[35] Langley, R. S., 2015, "Bounds on the Vibrational Energy That Can Be Harvested From Random Base Motion," J. Sound Vib., **339**, pp. 247–261.
[36] He, Q., and Daqaq, M. F., 2014, "Influence of Potential Function Asymmetries on the Performance of Nonlinear Energy Harvesters Under White Noise," ASME Paper No. DETC2014-34397.
[37] Oldham, K., and Spanier, J., 1974, *The Fractional Calculus Theory and Applications of Differentiation and Integration to Arbitrary Order*, Vol. 111, Elsevier, Amsterdam, The Netherlands.
[38] Torczon, V., 1997, "On the Convergence of Pattern Search Algorithms," SIAM J. Optim., **7**(1), pp. 1–25.
[39] Lewis, R. M., and Torczon, V., 1999, "Pattern Search Algorithms for Bound Constrained Minimization," SIAM J. Optim., **9**(4), pp. 1082–1099.
[40] Audet, C., and Dennis, J. E., Jr, 2002, "Analysis of Generalized Pattern Searches," SIAM J. Optim., **13**(3), pp. 889–903.
[41] Psaros, A. F., Brudastova, O., Malara, G., and Kougioumtzoglou, I. A., 2018, "Wiener Path Integral Based Response Determination of Nonlinear Systems Subject to Non-White, Non-Gaussian, and Non-Stationary Stochastic Excitation," J. Sound Vib., **433**, pp. 314–333.
[42] Meimaris, A. T., Kougioumtzoglou, I. A., Pantelous, A. A., and Pirrotta, A., 2019, "An Approximate Technique for Determining in Closed Form the Response Transition Probability Density Function of Diverse Nonlinear/Hysteretic Oscillators," Nonlinear Dyn., **97**(4), pp. 2627–2641.
[43] Psaros, A. F., Petromichelakis, I., and Kougioumtzoglou, I. A., 2019, "Wiener Path Integrals and Multi-Dimensional Global Bases for Non-Stationary Stochastic Response Determination of Structural Systems," Mech. Syst. Signal Process., **128**, pp. 551–571.
[44] Naess, A., and Johnsen, J., 1993, "Response Statistics of Nonlinear, Compliant Offshore Structures by the Path Integral Solution," Probab. Eng. Mech., **8**(2), pp. 91–106.
[45] Di Paola, M., and Santoro, R., 2008, "Path Integral Solution for Non-Linear System Enforced by Poisson White Noise," Probab. Eng. Mech., **23**(2–3), pp. 164–169.
[46] Chaichian, M., and Demichev, A., 2001, *Path Integrals in Physics: Stochastic Processes and Quantum Mechanics*, Institute of Physics Publishing, Bristol, UK.
[47] Nocedal, J., and Wright, S., 2006, *Numerical Optimization* (Springer Series in Operations Research and Financial Engineering), Springer, New York.

[48] Byrd, R. H., Gilbert, J. C., and Nocedal, J., 2000, "A Trust Region Method Based on Interior Point Techniques for Nonlinear Programming," Math. Program., **89**(1), pp. 149–185.
[49] Waltz, R. A., Morales, J. L., Nocedal, J., and Orban, D., 2006, "An Interior Algorithm for Nonlinear Optimization That Combines Line Search and Trust Region Steps," Math. Program., **107**(3), pp. 391–408.
[50] Kumar, P., Narayanan, S., Adhikari, S., and Friswell, M., 2014, "Fokker–Planck Equation Analysis of Randomly Excited Nonlinear Energy Harvester," J. Sound Vib., **333**(7), pp. 2040–2053.
[51] He, Q., and Daqaq, M. F., 2015, "New Insights Into Utilizing Bistability for Energy Harvesting Under White Noise," ASME J. Vib. Acoust., **137**(2), p. 021009.